IGBT-SiC Dual Fed Open End Winding PMSM Drive

Luca Rovere[1], Andrea Formentini[2], Giovanni Lo Calzo[3], Tom, Cox[4], Pericle Zanchetta[5]
[1] Department of Electrical and Electronic Engineering, The University of Nottingham, Nottingham, U.K., luca.rovere@nottingham.ac.uk
[2] Department of Electrical and Electronic Engineering, The University of Nottingham, Nottingham, U.K.
[3] Department of Electrical and Electronic Engineering, The University of Nottingham, Nottingham, U.K.
[4] Department of Electrical and Electronic Engineering, The University of Nottingham, Nottingham, U.K.
[5] Department of Electrical and Electronic Engineering, The University of Nottingham, Nottingham, U.K.

***Abstract*— This paper proposes a dual fed common dc link inverter Open End Winding-Permanent Magnet Synchronous Motor (OEW-PMSM) Drive. In order to increase the system efficiency a dual technology converter is used, with one inverter composed of standard IGBT devices and the other composed of fast switching Silicon Carbide (SiC) devices. The common dc link OEW configuration allows the zero-sequence current (ZSC) to flow freely, and the low time constants of the zero-circuit can lead to high zero sequence current flow, with associated losses and stress on the power devices. To avoid this, the zero-sequence voltage produced by the switching combinations adopted to synthetize the control signals needs to be instantaneously eliminated. A novel modulation for dual converter configurations is proposed to eliminate the zero-sequence voltage(ZSV).**

Keywords*— *Dual Inverter Drive, open end winding, permanent magnet synchronous motor, Wide bandgap devices, Silicon Carbide Technology, zero/sequence current

I. INTRODUCTION

PMSM are widely used in both academic and industrial applications[1-3]. The OEW-PMSM configuration offers several advantages in the field of variable-speed ac drives. It combines the high efficiency, high performance, compact construction and high torque per volume ratio of the PMSMs with the high fault tolerant capabilities, the multilevel modulation effect[4] and the reduction by half of the dc bus voltage of the OEW configuration. Two isolated dc power supplies[5], one dc supply and a floating bridge or a single dc supply[6] can be adopted for the dual inverter OEWM. Even though the first two solutions can be employed to avoid zero-sequence current (ZSC) circulation, still the ZSV due to the switching can produce shaft voltage and bearing currents[7, 8]. While on one hand the common dc bus configuration significantly simplifies and reduces the costs of the topology, on the other hand it allows the ZSC to flow freely in the system[9]. The circulation of additional current increases the losses and reduces the system efficiency, but the level of ZSC developed depends on the zero-sequence inductance magnitude[10]. The zero-sequence inductance coincides with the leakage inductance of the machine which is generally kept low (4-7% of the phase inductance) since it does not increase the average torque produced. Small time constants of the zero-sequence circuit produce a high frequency, high intensity current ripple with the risk of harming the switching devices. Hence particular attention needs to be given to the zero-sequence impedance when a machine is operated in OEW configuration. The most critical implementation of the OEW configuration happens when small phase inductance machines are used, leading to high ZSC circulation. SiC technology in combination with standard IGBT devices can be used to increase the system efficiency as demonstrated in [11]. The SiC devices can work at higher frequencies than the conventional IGBT with less switching losses. Since the upper current limit for SiC devices is lower than for IGBT devices, it is challenging to use them in the same topology. The OEW configuration with a common dc link allows the use of double the supply voltage in order to halve the supply current for constant power. In this paper a new mixed technology composed of two converters, IGBT and SiC, feeding an OEWM is used in order to obtain higher system efficiency and reduce the zero-sequence circulating current problem. A new modulation for the proposed architecture united with a zero-sequence current instantaneous elimination strategy is presented.

II. OEW PMSM MODEL

Fig. 1 shows the OEWM supplied at each end respectively by the SiC converter and the IGBT one. The mathematical model of the OEW-PMSM can be obtained from the well-known star connected one where the neutral point of the stator windings is opened. When working with the OEW configuration supplied from a single dc link it is necessary to take into account that the sum of the phase currents is no longer zero, but equal to the neutral current i_n

$$i_a + i_b + i_c = i_n \tag{1}$$

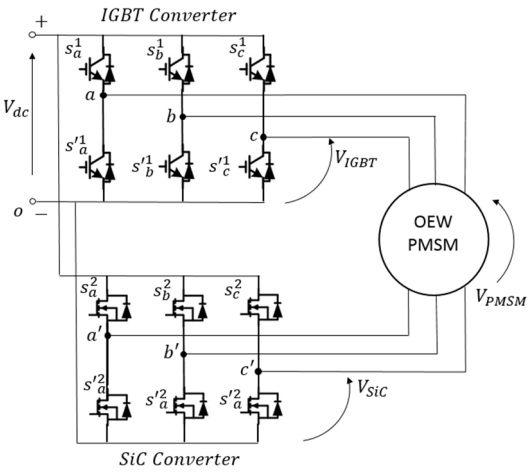

Fig. 1 Dual Fed IGBT-SiC OEW PMSM Drive

For the general case of a salient OEW-PMSM where the magnetic saturation is neglected and perfect sinusoidal EMFs are considered the machine voltage equations are:

$$\begin{bmatrix} V_{aa'} \\ V_{bb'} \\ V_{cc'} \end{bmatrix} = \begin{bmatrix} R_s & 0 & 0 \\ 0 & R_s & 0 \\ 0 & 0 & R_s \end{bmatrix} \begin{bmatrix} i_a \\ i_b \\ i_c \end{bmatrix} + \frac{d}{dt} \begin{bmatrix} \varphi_a \\ \varphi_b \\ \varphi_c \end{bmatrix} \quad (2)$$

$$\begin{bmatrix} \varphi_a \\ \varphi_b \\ \varphi_c \end{bmatrix} = [L_{abc}] \begin{bmatrix} i_a \\ i_b \\ i_c \end{bmatrix} + \phi_m \begin{bmatrix} sin(\vartheta_e) \\ sin(\vartheta_e - \frac{2}{3}\pi) \\ sin(\vartheta_e + \frac{2}{3}\pi) \end{bmatrix} \quad (3)$$

Where $V_{aa'}$, $V_{bb'}$ and $V_{cc'}$ are the phase voltages, φ_a, φ_b and φ_c are the flux linkages, $R_s, \vartheta_e, \omega_e$ and ϕ_m are respectively the stator resistance, electrical position, electrical speed and flux linkage while $[L_{abc}]$ is the stator inductance matrix as shown in (4-6)

$$[L_{abc}] = \begin{bmatrix} L_{11} & L_{12} & L_{13} \\ L_{21} & L_{22} & L_{23} \\ L_{31} & L_{32} & L_{33} \end{bmatrix} \quad (4)$$

$$\begin{cases} L_{11} = L_{ls} + L_A + L_B cos(2\vartheta_r) \\ L_{12} = L_{21} = -L_A + L_B\, cos(2\vartheta_r - \frac{2}{3}\pi) \\ L_{13} = L_{31} = -L_A + L_B\, cos(2\vartheta_r + \frac{2}{3}\pi) \\ L_{22} = L_{ls} + L_A + L_B cos(2\vartheta_r - \frac{2}{3}\pi) \\ L_{23} = L_{32} = -L_A + L_B\, cos(2\vartheta_r + 2\pi) \\ L_{33} = L_{ls} + L_A + L_B cos(2\vartheta_r + \frac{2}{3}\pi) \end{cases} \quad (5)$$

$$\begin{cases} L_A = \frac{L_d + L_q}{3} \\ L_B = \frac{L_q - L_d}{3} \end{cases} \quad (6)$$

Where L_A is the constant term of the phase inductance and L_B is the term that takes into consideration the anisotropy of the rotor, $L_q$and L_d are the q- and d- axis inductances while L_{ls} is the phase leakage inductance. The model in the rotor reference frame can be obtained by means of the Park transformation as

$$\begin{bmatrix} V_q \\ V_d \\ V_0 \end{bmatrix} = \begin{bmatrix} R_s & \omega_e L_d & 0 \\ -\omega_e L_q & R_s & 0 \\ 0 & 0 & R_s \end{bmatrix} \begin{bmatrix} i_q \\ i_d \\ i_0 \end{bmatrix} + \begin{bmatrix} L_q + L_{ls} & 0 & 0 \\ 0 & L_d + L_{ls} & 0 \\ 0 & 0 & L_{ls} \end{bmatrix} \frac{d}{dt} \begin{bmatrix} i_q \\ i_d \\ i_0 \end{bmatrix} + \begin{bmatrix} \omega_e \phi_m \\ 0 \\ 0 \end{bmatrix} \quad (7)$$

Where the leakage inductance L_{ls} will be renamed as the zero-sequence inductance L_0. During the machine design process the zero-sequence inductance is kept as low as possible because it does not contribute to any increment of the average torque produced, as can be seen from torque equation (8).

$$T_e = \frac{3}{2} p(\phi_m i_q + (L_d - L_q) i_d + 6\phi_{3m} cos(3\vartheta_e) i_0) \quad (8)$$

Where p is the number of pole pairs and ϕ_{3m} is the third harmonic amplitude of the flux linkage established by the magnets. When the machine back electromagnetic force is not perfectly sinusoidal an oscillation at 3 times the fundamental frequency with zero mean is added to the electromagnetic torque due to the flow of a ZSC. Higher L_0 would also correspond to a less efficient machine. For these reasons generally the leakage inductance is kept low (common values are around the 5% of the phase inductance). Therefore the value of the zero-sequence inductance depends on the machine parameters and is significantly smaller than the phase inductance[10, 12, 13]. In the particular case of high speed or high power machines, the value of the zero-sequence inductance is very small due to a small phase inductance. Considering the third row of (7) the zero-sequence equivalent circuit for a dual fed OEWM is shown in Fig. 2. If the zero-sequence inductance has a small value, the time constant of the equivalent RL circuit is too fast making the zero current difficult to be controlled and, in most cases, the zero current switching ripple inacceptable. In fact 1/3 of the zero sequence current is summed to each phase current as additional ripple that would not only reduce the quality of the waveforms produced but especially increase the stress for the power switching devices of the converter. When the machine is used in OEW architecture its parameters need to be taken into account in order to understand the zero-sequence current ripple and evaluate if it is tolerable or if the current needs to be suppressed.

III. Dual-Fed IGBT SiC OEW-PMSM Drive

A. Dual Inverter Voltage Vectors

From Fig. 1 the phase voltages of the dual fed OEW Drive with common dc link as a function of the switching states are:

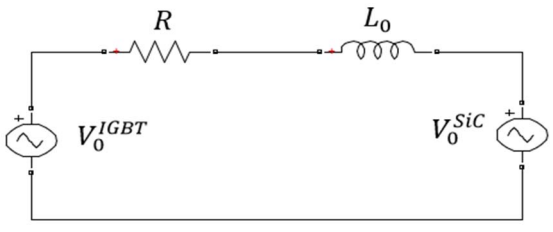

Fig. 2 Zero-sequence equivalent circuit

$$\begin{bmatrix} V_{aa'} \\ V_{bb'} \\ V_{cc'} \end{bmatrix} = \begin{bmatrix} s_a^1 - s_a^2 \\ s_b^1 - s_b^2 \\ s_c^1 - s_c^2 \end{bmatrix} V_{dc} \qquad (9)$$

Where s_k^h indicates the switching state of the inverter and it can be equal to 1 if the switch device on the upper bridge turns on or 0 is the switch device on the lower bridge turns on. Subscript k indicates the phase while superscript h stands for the IGBT converter when equal to 1 or the SiC converter when equal to 2. In the stationary αβ0 coordinate frame the phase voltages of (2) can be expressed as (10).

$$\begin{bmatrix} V_\alpha \\ V_\beta \\ V_0 \end{bmatrix} = \frac{2}{3} \begin{bmatrix} 1 & -\frac{1}{2} & -\frac{1}{2} \\ 0 & \frac{\sqrt{3}}{2} & -\frac{\sqrt{3}}{2} \\ \frac{1}{2} & \frac{1}{2} & \frac{1}{2} \end{bmatrix} \begin{bmatrix} V_{aa'} \\ V_{bb'} \\ V_{cc'} \end{bmatrix} \qquad (10)$$

It follows that there are 8 x 8 = 64 possible combinations of switching states: they are possible realisations of 19 different space voltage vectors of which 18 are different active vectors corresponding to the vertices of the two green hexagons and the red dotted one of Fig. 3, and 1 zero vector located at the origin. It should be noted that this configuration provides a number of different space voltage vectors equal to the one of a three-level inverter. However, if the machine leakage inductance is too small, all the vectors that generate a non-zero V_0 cannot be used to avoid the presence of a big zero-sequence ripple. The number of admissible switching states that can be used to synthetize the voltage control actions are the ones with zero V_0 component. The 64 switching states reduce than to 20: they can produce 1 zero vector at the origin and 6 different active vectors corresponding to the vertexes of the red dashed hexagon of Fig. 3. Each hexagon of Fig. 3 Space voltage vectors of the dual inverterFig. 3 has a maximum linear modulation index associated where the modulation index m is defined as

$$m = \frac{|V|}{V_{dc}} \qquad (11)$$

Where V is the reference voltage aimed to be synthetized by the inverter and V_{dc} is the dc-link voltage. Always referring to

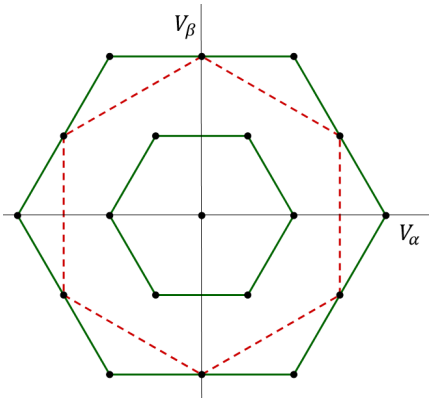

Fig. 3 Space voltage vectors of the dual inverter

Fig. 3 the maximum linear modulation indexes are $1/\sqrt{3}$, 1 and $2/\sqrt{3}$ for the small hexagon, the dotted red one and the big green one respectively. Working with space vectors with no ZSV corresponds to work on the red dotted hexagon thus having a reduction of 13.4% compared to the maximum modulation index (m) that this double converter configuration would allow. The dc-link utilisation is still higher if compared with a standard single VSI drive (corresponding to the small green hexagon) gaining 42.3%.

B. Duty Cycles generation for Dual-Fed IGBT-SiC OEW-PMSM Drive

In order to exploit the different nature of the two technologies used in the two converters a new way to generate the duty cycles for the two bridges of the dual-fed architecture is presented. From Fig. 1 it is clear how the voltage on the OEWM is the difference between the IGBT converter output voltage and the SiC one

$$V_{PMSM} = V_{IGBT} - V_{SiC} \qquad (12)$$

In the dual-fed single dc-link configuration the maximum and minimum voltage that can be applied to each phase of the OEWM are V_{dc} and $-V_{dc}$ respectively compared to $V_{dc}/2$ and $-V_{dc}/2$ of a standard single VSI drive. The modulation duty cycles are obtained normalising the FOC output waveforms with respect to V_{dc}. The new modulation technique proposed is based on the voltage equation (12), in fact the same relationship is used for duty cycle generation for the IGBT and SiC converters that will be fed to the modulators

$$d_{abc} = d_{IGBT} - d_{SiC} \qquad (13)$$

Where d_{abc} are the duty cycles corresponding to the normalised FOC output control voltages, d_{IGBT} and d_{SiC} are respectively the duty cycles of the IGBT and SiC converters. As already mentioned the aim is to exploit the two different technologies used for the two converters with the intent to reduce the overall converter losses, therefore the IGBT modules switch at the lowest possible switching frequency while the SiC is intended to switch as fast as possible. Setting the IGBT converter to modulate in six-step mode, i.e. square wave mode at the fundamental frequency of the FOC output waveforms would result in extremely low switching frequency and almost exclusively conduction losses for the IGBT switching devices. E.g. if we consider a 3 pole pairs OEWM rotating at 3000 rpm the IGBT converter switching frequency would be 150 Hz. The IGBT duty cycles are then obtained from the FOC ones as follows

$$d_{IGBT} = 0.5\, sign(\, d_{abc}\,) \qquad (14)$$

From (14) the IGBT duties consists in 3 square waveforms of amplitude 0.5 with the same phase displacement of the 3 modulating FOC d_{abc} signals. The modulating signals for the SiC converter are obtained from (13) knowing that the IGBT ones are expressed by (14) as

$$d_{SiC} = \begin{cases} (0.5 - d_{abc}) & if\ d_{abc} > 0 \\ (-0.5 - d_{abc}) & if\ d_{abc} < 0 \end{cases} \quad (15)$$

The modulation described in (13-15) consists of a square wave control of the IGBT converter allowing it to switch at the fundamental frequency set by the motor speed. The square wave modulation of the IGBT converter introduces elevated harmonic distortion therefore the SiC converter needs to switch faster than the IGBT one in order to compensate it. The role of the SiC converter in this configuration can be interpreted as an active filter that eliminates the harmonic distortion introduced by the low switching IGBT one. This separation of the duty cycles between the two converters results in an increased efficiency of the overall architecture and allows exploitation of the different natures of the two converters. Considering the different switching frequencies of the two converters the IGBT is mainly responsible for the conduction losses while the SiC is responsible for the switching losses. The flowchart of the proposed modulation strategy is shown in Fig. 4.

C. *Suppression of Zero-Sequence Current in Dual-Fed IGBT SiC OEW-PMSM Drive*

Even if the common dc-link configuration presents the advantages of reducing the costs of the supply it still presents the drawback of circulating currents through the converters and the OEWM. As already mentioned the drawbacks of ZSC flowing into the drive would result not only in higher losses but also in a significant phase current ripple due to the low time constant of the zero-sequence circuit. Therefore in order not to excite the equivalent zero-sequence circuit of Fig. 2 the ZSVs produced by the two converters must be instantaneously the same. The zero-sequence current can be instantaneously eliminated by modulating at each sample time a ZSV V_0 equal to 0. That means by looking at Fig. 2 to have the common mode voltage produced by the square wave modulated IGBT converter equal to the common mode voltage generated by the SiC converter. Fig. 5 shows the duty cycle waveforms of the proposed modulation while their corresponding trajectories in the αβ plane are shown in Fig. 6. The values that the ZSV V_0 assumes for each inverter state should be presented as a third dimension perpendicular to the αβ plane but for simplicity of comprehension it has been added as a label next to the inverter state in Fig. 6. The blue hexagon of Fig. 6 corresponds to the square wave IGBT duty modulation while the red trace corresponds to the duty cycle modulation for the SiC converter. The two black triangles are obtained from connecting the vertices of the voltage state vectors with the same ZSV. Furthermore the values assumed by the 8 state vectors for a single VSI in the abc and αβ coordinates normalised in respect to $V_{dc}/2$ are reported in Table I for clarity of explanation. Considering the single inverter, either the IGBT or the SiC one it can be noticed form Table I that for the 6 active vectors V_{1-6} the ZSV V_0 can be either $\frac{V_{dc}}{6}$ or $-\frac{V_{dc}}{6}$. Hence the square wave duty cycles for the IGBT converter in the alpha beta plane corresponds to jumping from one inverter state to the adjacent $(V_1, V_2, \dots, V_6)$ never passing from the zero state vectors V_0 and V_7, therefore the ZSV of the IGBT converter is also a square wave of amplitude $\frac{V_{dc}}{6}$. By adopting a conventional triangular wave PWM for the SiC converter the resulting V_0 on the OEW-PMSM would not be instantaneously equal to 0. A new modulation for the SiC inverter is developed in order to instantaneously set V_0 to zero. Considering again Fig. 6 it is clear that when the IGBT is on the states V_1, V_3 and V_5 the ZSV generated is $-\frac{V_{dc}}{6}$, hence, considering voltage equation (11) to obtain zero ZSV on the PMSM also the SiC has to be $-\frac{V_{dc}}{6}$. In order to obtain so the SiC converter needs to modulate only between V_1, V_3 and V_5. The same applies for the states V_2, V_4 and V_6. When the IGBT square wave modulation is applying any of the vectors V_2, V_4 and V_6 the ZSV produced by the converter is $\frac{V_{dc}}{6}$, therefore also the SiC converter needs to produce the same ZSV that corresponds to modulation between the states V_2, V_4 and V_6. The SiC modulating duty cycles represented in the alpha-beta plane will be then modulated with the odd vectors when the IGBT is on one of the odd vectors and with even states when the IGBT is on even states. The SiC converter modulation states are represented by the two black triangles of Fig. 6, one triangle has the vertices coinciding with the states with $\frac{V_{dc}}{6}$ of ZSV while the other with $-\frac{V_{dc}}{6}$. The overall control structure of the system is shown in Fig. 7. Thanks to the zero-sequence current modulation introduced to synthetize the SiC reference duty cycles the zero- sequence PI controller is not needed since at each sample time the ZSV of the SiC inverter is equal to the ZSV of the IGBT converter.

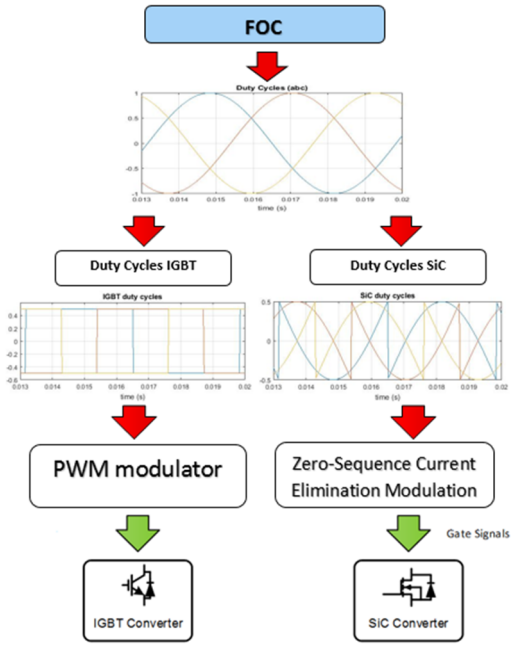

Fig. 4 Duty cycles generation flowchart

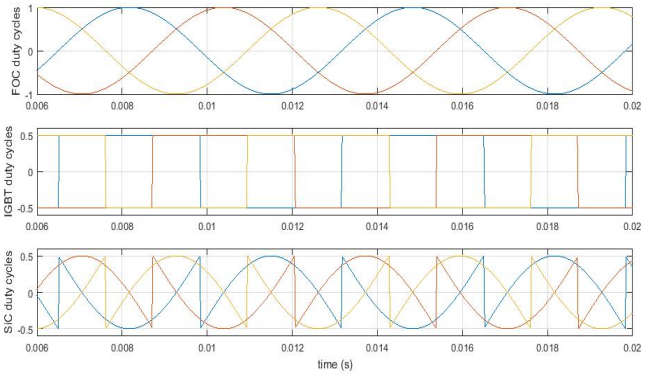

Fig. 5 Duty cycles waveforms. Stating from top: FOC duties, IGBT duties, SiC duties.

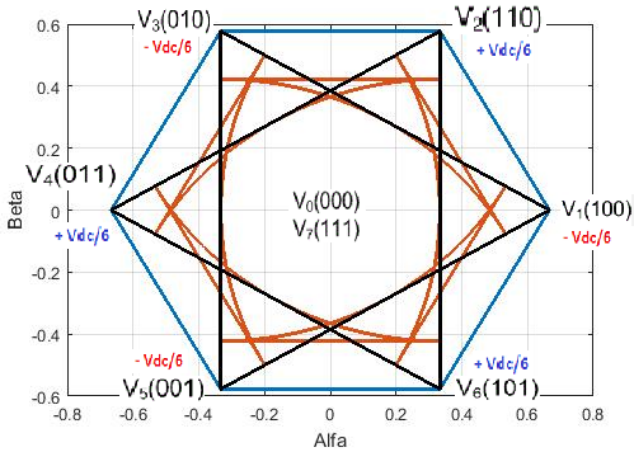

Fig. 6 Converters Duty cycles trajectories on the αβ plane.

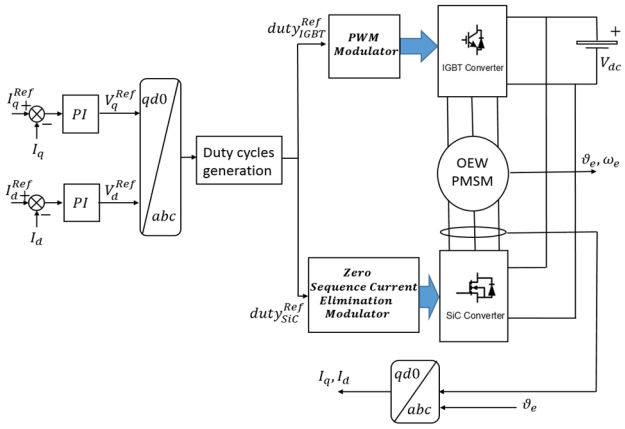

Fig. 7 Proposed control structure fot the IGBT-SiC OEW-PMSM

IV. Simulation Results

The performance of the proposed drive has been tested in simulation using Matlab\Simulink. The system parameters used are listed in Table II. The results included in this paper are obtained by implementing the drive torque control loop with reference current values externally imposed. The reference rotor speed is imposed as if the motor speed was controlled by an external machine. Fig. 8 and Fig. 9 show the simulation results when standard PWM modulation for both converters is used. In particular Fig. 8 shows the ZSV for the IGBT and SiC converters while Fig. 9 shows the resulting ZSV on the OEW-PMSM and the phase currents, it can be noticed that the ZSV produced by the SiC converter is different from the square wave ZSV of the IGBT, consequently the zero circuit is excited and the ZSC is responsible of the high intensity ripple of the phase currents. Fig. 10 and Fig. 11 show the ZSVs for the IGBT, SiC converters, the OEW-PMSM and the phase current behaviour when the zero sequence cancellation modulation is implemented. The SiC ZSV is now modulated to be equal to the one produced by the IGBT at each sample time, removing ZSV on the OEW-PMSM and significantly reducing the phase current ripple.

V. Conclusions

In this paper a new mixed technology IGBT-SiC Dual-fed OEW-PMSM Drive united with a zero-sequence current suppression strategy is presented. The adopted modulating technique splits the FOC between the two converters, taking advantage of the two different technologies used and resulting in high efficiency of the overall system. In depth discussion of the zero-sequence current impact and its dependence from the machine parameters in order to evaluate if it is acceptable has been carried out. Furthermore the modulation for zero-sequence current instantaneous suppression has been presented.

TABLE I SINGLE INVERTER VOLTAGE STATES

		V_α	V_β	V_0
V_0	[0 0 0]	0	0	$-1/2$
V_1	[1 0 0]	$2/3$	0	$-1/6$
V_2	[1 1 0]	$1/3$	$-1/\sqrt{3}$	$1/6$
V_3	[0 1 0]	$-1/3$	$-1/\sqrt{3}$	$-1/6$
V_4	[0 1 1]	$-2/3$	0	$1/6$
V_5	[0 0 1]	$-1/3$	$1/\sqrt{3}$	$-1/6$
V_6	[1 0 1]	$1/3$	$1/\sqrt{3}$	$1/6$
V_7	[1 1 1]	0	0	$1/2$

TABLE II SIMULATION PARAMETERS

Name	Description	Value	Unit
R_s	Stator phase resistance	0.3	[Ω]
$L_q = L_d$	Stator inductance	1.2	[mH]
L_0	Zero-Sequence Inductance	75	[μH]
ϕ_m	Flux linkage established by magnets	0.060733	[V s]
p	Pole pairs	3	-

References

[1] A. Formentini, L. de Lillo, M. Marchesoni, A. Trentin, P. Wheeler, and P. Zanchetta, "A new mains voltage observer for PMSM drives fed by matrix converters," *in EPE*, 2014, pp. 1-10.

[2] A. Formentini, G. Maragliano, M. Marchesoni, and L. Vaccaro, "A sensorless PMSM drive with inductance estimation based on FPGA," *in SPEEDAM*, 2012, pp. 1039-1044.

[3] L. R. A. F. A. G. P. Z. M. Marchesoni, "Sensorless Finite Control Set Model Predictive Control for IPMSM Drives," *IEEE Transactions on Industrial Electronics* 8 Jun. 2016.

[4] H. Stemvmler, and P. Guggenbach, "Configurations of high-power voltage source inverter drives," *in Proc. EPE Conf.*, 1993, pp. 7-14.

[5] M. Narimani, and G. Moschopoulos, "Three-Phase Multimodule VSIs Using SHE-PWM to Reduce Zero-Sequence Circulating Current," vol. 61, no. 4, pp. 1659-1668, Apr. 2014.

[6] V. T. Somasekhar, K. Gopakumar, and M. R. Baiju, "Dual two-level inverter scheme for an open-end winding induction motor drive with a single DC power supply and improved DC bus utilisation," *Proc.Inst.Elect. Power Appl.*, vol. 151, no. 2, pp. 230-238, Mar. 2004.

[7] M. R. Baiju, K. K. Mohapatra, R. S. Kanchan, and K. Gopakumar, "A dual two-level inverter scheme with common mode voltage elimination for an induction motor drive," *IEEE Trans. Power Electron.*, vol. 19, no. 3, pp. 794-805, May 2004.

[8] J. Kalaiselvi, and S. Srinivas, "Bearing Currents and Shaft Voltage Reduction in Dual-Inverter-Fed Open-End Winding Induction Motor With Reduced CMV PWM Methods," vol. 62, no. 1, pp. 144-152, Jan. 2015.

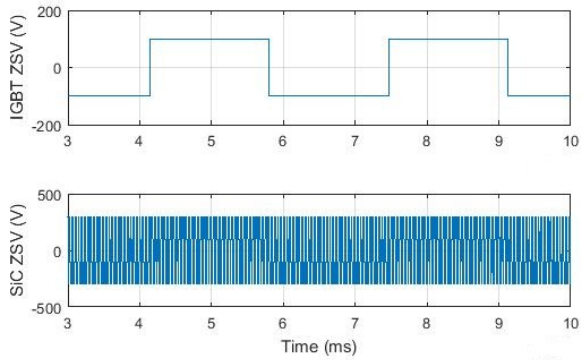

Fig. 8 Simulation results with ZSC flowing. Top: IGBT ZSV. Bottom: SiC ZSV.

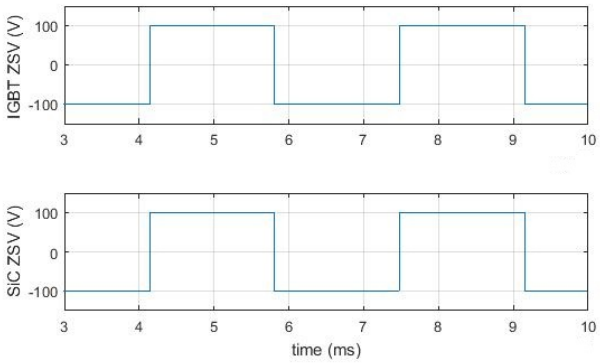

Fig. 10 Simulation results with ZSC elimination modulation. Top: IGBT ZSV. Bottom: SiC ZSV.

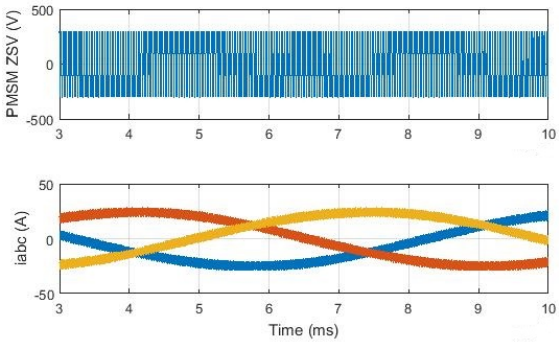

Fig. 9 Simulation results with ZSC flowing. Top: OEW-PMSM ZSV. Bottom: phase currents.

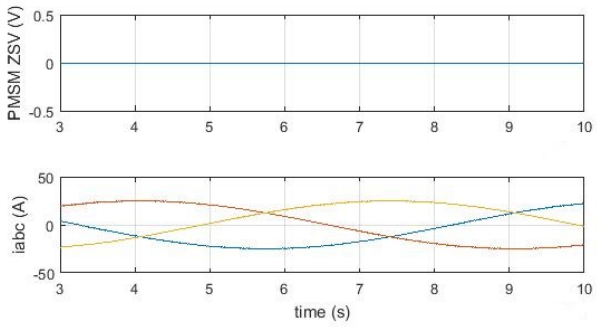

Fig. 11 Simulation results with ZSC elimination modulation. Top: OEW- PMSM ZSV. Bottom: phase currents.

[9] A. Somani, R. K. Gupta, K. K. Mohapatra, and N. Mohan, "On the Causes of Circulating Currents in PWM Drives With Open-End Winding AC Machines," *IEEE Trans. on Industrial Electronics,* vol. 60, no. 9, pp. 3670 - 3678, Sept. 2013.

[10] P. Sandulescu, F. Meinguet, X. Kestelyn, E. Semail, and A. Bruyere, "Control Strategies for Open-End Winding Drives Operating in the Flux-Weakening Region," vol. 29, no. 9, pp. 4829-4842, Sep. 2014.

[11] G. Lo Calzo, P. Zanchetta, C. Gerada, A. Gaeta, and F. Crescimbini, "Converter topologies comparison for more electric aircrafts high speed Starter/Generator application," *in IEEE Energy Conversion Congress and Exposition (ECCE)*, Montreal, QC, 2015.

[12] Q. An, J. Liu, Z. Peng, L. Sun, and L. Sun, "Dual-Space Vector Control of Open-End Winding Permanent Magnet Synchronous Motor Drive Fed by Dual Inverter," *IEEE Trans. on Power Electronics,* vol. 31, no. 12, pp. 8329 - 8342, 2016.

[13] T. S. Veeramraju, S. Srinivas., and K. K. Kumar., "Effect of Zero-Vector Placement in a Dual-Inverter Fed Open-End Winding Induction-Motor Drive With a Decoupled Space-Vector PWM Strategy," *IEEE Trans. Ind Electr.,* vol. 55, no. 6, pp. 2497-2505, June 2008.